Neurobiology of Disease 129 (2019) 195–207

Contents lists available at ScienceDirect

Neurobiology of Disease

journal homepage: www.elsevier.com/locate/ynbdi

Dysregulated autophagy as a new aspect of the molecular pathogenesis of Krabbe disease☆

Ambra Del Grosso[a], Lucia Angella[a], Ilaria Tonazzini[a], Aldo Moscardini[a], Nadia Giordano[b,c], Matteo Caleo[c,d], Silvia Rocchiccioli[e], Marco Cecchini[a,*]

[a] NEST, Isituto Nanoscienze-CNR and Scuola Normale Superiore, Piazza San Silvestro 12, 56127 Pisa, Italy
[b] Scuola Normale Superiore, Piazza dei Cavalieri 7, 56127 Pisa, Italy
[c] CNR Neuroscience Institute, via G. Moruzzi 1, 56124 Pisa, Italy
[d] Department of Biomedical Sciences, University of Padua, 35121 Padova, Italy
[e] Institute of Clinical Physiology-CNR, Via Giuseppe Moruzzi 1, Pisa 56124, Italy

ARTICLE INFO

Keywords:
Globoid cell leukodystrophy
GLD
Krabbe disease
KD
Autophagy
Psychosine
PSY
p62
Rapamycin
Lysosomal storage disorders
LSD

ABSTRACT

Krabbe disease (KD) is a childhood leukodystrophy with no cure currently available. KD is due to a deficiency of a lysosomal enzyme called galactosyl-ceramidase (GALC) and is characterized by the accumulation in the nervous system of the sphingolipid psychosine (PSY), whose cytotoxic molecular mechanism is not fully known yet.

Here, we study the expression of some fundamental autophagy markers (LC3, p62, and Beclin-1) in a KD murine model [the twitcher (TWI) mouse] by immunohistochemistry and Western blot. Moreover, the autophagy molecular process is also shown in primary fibroblasts from TWI and WT mice, with and without PSY treatment. Data demonstrate that large p62 cytoplasmic aggregates are present in the brain of both early and late symptomatic TWI mice. p62 expression is also upregulated in TWI sciatic nerves compared to that measured for WT nerves. *In vitro* data suggest that this effect might not be fully PSY-driven. Finally, we investigate *in vitro* the capability of autophagy inducers (Rapamycin, RAP and Resveratrol, RESV) to reinstate the WT phenotype in TWI cells. We show that RAP administration can partially restore the autophagy markers levels, while RESV cannot, indicating a line along which new therapeutic approaches can be developed.

1. Introduction

Krabbe disease (KD or globoid cell leukodystrophy, GLD) is a rare, hereditary and neurodegerative disorder, triggered by a deficit of the lysosomal enzyme galactosylceramidase (GALC) and characterized by the accumulation of galactosylsphingosine (psychosine, PSY) in the nervous system (Esch et al., 2003; Whitfield et al., 2001). PSY is a cytotoxic sphingolipid, which leads to the widespread degeneration of oligodendrocytes and Schwann cells, causing demyelination. Still, little is known about the molecular mechanisms by which PSY imparts toxicity and there is currently no cure available for KD. The early-infantile and most widespread form of this lysosomal storage disorder (LSD) is rapidly progressive and lethal. Bone marrow transplantation (BMT) is presently the only clinically applied method to treat KD, but gene therapy has yielded good results in several experimental models (Mikulka and Sands, 2016). However, the recent literature strongly suggests that GALC-deficiency correction is not sufficient to completely rescue the KD phenotype (Rafi et al., 2015; Ricca et al., 2015). Thus, supportive therapies specifically addressing secondary targets of the disease might be needed to improve the final therapeutic outcome.

Autophagy is a dynamic degradation pathway by which cytosolic material, including damaged organelles, proteins, carbohydrates, lipids and pathogens, are delivered to the lysosome for degradation. The initiation phase of the autophagy pathway is finely regulated by several proteins that form regulatory initiation complexes. One of the most studied protein is, for example, Beclin-1, that presents three different structural domains interacting with a wide network of proteins involved in the regulation of the autophagy machinery. In particular, interacting with several cofactors, Beclin-1 regulates the lipid kinase Vps-34 promoting the formation of the Beclin-1-Vps34-Vps15 core complex,

☆ All authors had full access to all the data in the study and take responsibility for the integrity of the data and the accuracy of the data analysis. Study concept and design: ADG, LA, MCecc. Acquisition of data: ADG, LA, NG, AM, SR, IT. Analysis and interpretation of data: All authors. Drafting of the manuscript: All authors. Statistical analysis: ADG, LA, MCecc. Obtained funding: MCecc. Study supervision: MCecc.

* Corresponding author.
E-mail address: marco.cecchini@nano.cnr.it (M. Cecchini).

https://doi.org/10.1016/j.nbd.2019.05.011
Received 18 February 2019; Received in revised form 8 May 2019; Accepted 13 May 2019
Available online 17 May 2019

thereby inducing autophagy (Kang et al., 2011). Thus, after a specific trigger positive input, the process physically starts with the formation of double-membrane-layer vesicles called autophagosomes from cup-shaped structures (the phagophores). In this phase microtubule-associated protein 1 light-chain 3 (LC3) helps in phagophore edge folding and binds adaptor proteins (such as the ubiquitin-binding protein p62) that, in turn, can regulate the degradation of specific cellular and molecular structures, making autophagy a selective process. Subsequently, autophagosomes fuse with lysosomes, forming the so-called autolysosomes and allowing the final stage of autophagy in which the luminal material is degraded by the resident hydrolases.

LSDs are characterized by the accumulation of undigested macromolecules within the cell, and can show impaired autophagy features (Settembre et al., 2008a; Lieberman et al., 2012). However, very little is known about autophagy in KD; autophagy dysregulations have been only recently found in KD cellular models by us and others (Ribbens et al., 2014; Del Grosso et al., 2016). Furthermore, in the current literature autophagy has never been analysed in the most widely accepted murine model of KD, the twitcher (TWI) mouse (Duchen et al., 1980; Cappello et al., 2016; Pellegrini et al., 2019), except for a very recent study performed by Abdelkarim and collaborators (Abdelkarim et al., 2018). They demonstrated that PSY and α-synuclein colocalize in the lysosomal pathway in the TWI brain, and that TWI brains also show an elevated basal level of both LAMP-1 and LC3-I markers. α-synuclein is generally linked to the pathogenesis of Parkinson's disease (PD), but has just been recently found accumulated also in KD human and mouse brains (Abdelkarim et al., 2018; Smith et al., 2014; Marshall and Bongarzone, 2016).

Cytoplasmic aggregation-prone proteins causing neurodegeneration, such as α-synuclein, are in general good autophagy substrates and, besides LSDs, autophagy dysregulation is a well-known characteristic of the most common neurodegenerative disorders. Several molecules that accumulate in these disorders, such as PD, Alzheimer's (AD) and Huntington's (HD) diseases, revealed in fact to be autophagic substrates (Ballabio and Gieselmann, 2009). The accumulation of these aggregation-prone proteins, thus, saturates the autophagic flux ultimately blocking it, and not allowing their proper degradation. Thereby, up-regulation of autophagy is considered a therapeutic strategy for several neurodegenerative diseases (Sarkar et al., 2009; Rubinsztein et al., 2012; Fleming et al., 2011). The beneficial effects of autophagy up-regulation in neurodegenerative diseases first came with the mTOR inhibitor Rapamycin (RAP), which ameliorated the disease phenotype in transgenic HD mice (Ravikumar et al., 2004). Subsequently, RAP was protective in other various cellular and animal neurodegenerative models (Pan et al., 2008; Wang et al., 2009; Mandrioli et al., 2018). Later, lots of autophagy enhancers have been discovered and tested. Resveratrol (RESV), for example, can induce autophagy *via* an mTOR dependent pathway and was found to promote remyelination in a model of multiple sclerosis (Ghaiad et al., 2016). The discovery of mTOR-independent autophagy enhancers, such as Lithium (Li), a drug that has been used for decades to chronically treat people with affective disorders, also provided an alternative way to stimulate autophagy. In our previous work, we likewise demonstrated that Li can activate autophagy and, more interestingly, that this drug can partially restore cell viability in an immortalized cell model of oligodendrocytes after PSY administration (Del Grosso et al., 2016).

In this work, we investigate the expression of some fundamental autophagy markers, LC3, p62 and Beclin-1, in the TWI mouse, by immunohistochemistry and Western blot techniques. We also show the autophagy molecular process in primary fibroblasts from TWI and WT mice, with and without PSY treatment. By high-pressure liquid chromatography-mass spectrometry methods (HPLC/MS), we investigate whether the changes in autophagy marker levels that we found in TWI cells could be considered PSY-driven. Finally, in view of possible new therapeutic approaches to treat KD, we show the capability of two mTOR-dependent autophagy modulators (RAP and RESV) to rescue *in vitro* the WT phenotype.

2. Materials and methods

2.1. Animals

TWI heterozygous mice (TWI+/− C57BL6 mice; Jackson Labs), kindly donated by Dr. A. Biffi (San Raffaele Telethon Institute for Gene Therapy, Milan, Italy), were used as breeder pairs to generate homozygous TWI mice (TWI−/−, elsewhere abbreviated as TWI for simplicity). Animals were maintained under standard housing conditions and used according to the protocols and ethical guidelines approved by the Ministry of Health (Permit Number: CBS-not. 0517; approved the 4/1/2018). For genotyping purpose, mice genomic DNA was extracted from clipped tails by Proteinase K digestion and subsequent genomic DNA extraction (EUROGOLD Tissue-DNA Mini Kit, Euroclone), as previously done by us (Parlanti et al., 2017; de Vito et al., 2017; de Vito et al., 2014). The genetic status of each mouse was later determined from the genome analysis of the TWI mutation, as reported from Sakai and coworkers (Sakai et al., 1996). Both PND 20 and 30 TWI and WT animals were used for experiments, while the heterozygous littermates were retained for the colony maintenance. For immunohistochemistry experiments, 4 TWI and 4 WT mice were used (2 PND 20 and 2 PND 30 for each group). Surgical procedures for fresh organs extraction and for fixation were performed under urethane anesthesia (Sigma Aldrich, 0.8 ml/hg), and all efforts were made to minimize mice suffering.

2.2. Immunohistochemistry

TWI and WT deeply anesthetized mice were sacrificed by transcardial perfusion with phosphate buffer saline (PBS) and subsequently with paraformaldehyde (PFA) 4%. After perfusion, the brains were stored at 4 °C in a 4% PFA solution for at minimum 2 days. Consecutive coronal brain sections, 50 μm thick, were cut with a microtome (VT 1000 S, Leica BIOSYSTEM) at 0.50–2.10 mm from bregma. Sections were maintained at 4 °C in PBS until use. For the immunohistochemistry staining, sections were transferred in a 24 well cell culture plate (maximum of 3 sections per well) and incubated with blocking solution (3% bovine serum albumin, 0.3% TritonX-100 in PBS; 1 ml per well) for 1 h at room temperature (RT). Then, the blocking solution was removed and the primary antibody mix (1% BSA, 0.3% TritonX-100, antibody at the optimal dilution and PBS to reach 1 ml) was added to the well and left overnight at 4° under gentle shaking. We used the following antibodies: anti-p62 (ab56416 Abcam, 1:100), anti-LC3 (ab48394 Abcam, 1:200), anti-NeuN (ab104225 Abcam, 1:1000), anti-GFAP (ab7260 Abcam, 1:1000), anti-MBP (ab980 Merck Millipore, 1:500), anti-LAMP-1 (sc-20,011 Santa Cruz, 1:200) and anti-LAMP-1 (21997–1-AP Proteintech, 1:200). These primary antibodies have been validated in previous studies (Del Grosso et al., 2016; Fu et al., 2017; Lu et al., 2017; Spalletti et al., 2017; Floden and Combs, 2011). The next morning, primary antibody solution was removed and 3 washes with 1 ml of PBS were made (10 min each). Then, secondary antibody solution was added (BSA 1%, TritonX-100 0,3%, anti-mouse or anti-rabbit Alexa 647 1:1000, anti-mouse or anti-rabbit Alexa 488 1:000 and PBS to reach 1 ml total volume). After 2 h of incubation at RT other 3 washes with PBS were made. Sections were then stained with a Hoechst solution for 1 min and then mounted on SUPERFROST Microscope Slides (Thermo Scientific) with Vectashield Antifade Mounting Medium (VECTOR LABORATORIES). Finally, slides were sealed and stored at 4 °C until confocal imaging.

2.3. Cell culture and treatments

Adult mouse fibroblast cultures were obtained from WT and TWI ears, according to the protocol established in the laboratory of Dr. Evan Eichler (University of Washington, https://genome.ucsc.edu/ENCODE/

protocols/cell/mouse/Fibroblast_Stam_protocol.pdf) from mice that were less than six months old. Briefly, after anesthesia, mouse ears were extracted, washed with sterile water and cut into small pieces. All pieces were then collected in an Eppendorf tube and added with collagenase XI (C7657–100 mg; Sigma Aldrich) diluted in high glucose Dulbecco's Modified Eagle Medium (DMEM) (approximately 2.5 mg of collagenase −320 CDU- for 1 mouse). After 2 h of incubation at 37 °C the Eppendorf tube was centrifuged for 5 min at 200*g*, the supernatant was discarded and the pellet was washed with 2 ml of PBS and centrifuged again discarding the supernatant. Trypsin-EDTA 0.05% (59418C-100ML; Thermo Fisher Scientific) was then added to the tube and left 45 min at 37 °C. The tube was then centrifuged and the pellet was resuspended in the complete DMEM [high glucose DMEM supplemented with 10% of heat-inactivated fetal calf serum (FCS), 4 mM L-glutamine, 1% MEM Nonessential Amino Acids and 1% penicillin/streptomycin; all products were from GIBCO-Life Technologies)]. Obtained cells were thus divided pipetting up and down with a syringe, plated in a 60 mm cell Petri and incubated at 37 °C in a humidified atmosphere containing 5% CO_2. The day after, cells were washed and medium was replaced. After reaching confluence (approximately 3–4 days), cells (p0) were washed with 1 ml of PBS and split with a ratio of 1:2. Cells were cultured and used for experiments within the 10th passage *in vitro*. For treatments, WT and TWI fibroblast primary cells were plated in standard 6 well cell plates (300,000 cells per well, for the western blot experiments), in 60 mm cell plates (800,000 cells, for PSY quantification experiments) or in 12 mm WillCo dishes (70,000 cells, for immunocytochemistry). After 24 h, depending on the treatment, cells were pre-treated with RAP 100 nM (tlrl-rap 5 mg; InvivoGen) or RESV 100 μM (tlrl-resv 100 mg; InvivoGen) for 1 h and then administered with PSY 100 μM (P9256-1MG; Sigma Aldrich). For selected experiments, cells were also treated with bafilomycin (BAF; B1793-2UG; Sigma Aldrich) 200 nM for 4 h before cell lysis. PSY, RAP, BAF, and RESV were dissolved in dimethylsulfoxide (DMSO). Control cultures received the same quantity of DMSO, which never exceeded 0.6% *v*/v.

2.4. Immunocytochemistry

WT and TWI fibroblasts were grown and fixed for 20 min with 4% formaldehyde/4% sucrose in PBS at RT. Then, fixed cells were washed 3 times with PBS (10 min for each wash). After washes, cells were incubated with primary antibodies (anti-LC3 and anti-p62, see par. *Immunohistochemistry*) diluted in the GDB buffer (0.2% BSA, 0.5%Triton, 0.8 M NaCl, Phosphate buffer 30 mM with pH 7.4) (Tonazzini et al., 2015). After an overnight incubation at 4 °C in a humid chamber, samples plates were washed 3 times in PBS and the secondary antibodies mix was added [anti-rabbit alexa 555, anti-mouse alexa 488 and alexa Fluor Phalloidin 647 (A-31572, A-11029, A-22287; Thermo Fisher Scientific), diluted, respectively, 1:1000, 1:1000 and 1:40 in the GDB buffer]. After 1,5 h of incubation at RT, 3 washes with PBS and 1 with water (to remove salt) were performed. After drying, Vectashield mounting medium with DAPI (F6057-20ML; Sigma Aldrich) was added and plates were stored at 4 °C until usage.

2.5. Confocal microscopy and images analysis

Immunostained cells and brain sections were imaged with a laser scanning confocal microscope TCS SP2 (Leica Microsystems) equipped with a 63× oil objective and interfaced with UV, Ar, HeNe and He lasers for excitation at 405, 488, 561 and 633 nm, respectively. Each reported confocal image was obtained from a z-series (stack depth was maximum 10 μm with steps of 0.5–1 μm for cells and maximum 20–30 μm with steps of 2 μm for brain sections).

The resulting z-stack was processed in ImageJ (NIH; RRID:SCR_003070) into a single image by using "z-project" and "Max intensity" options. The processed z-stack was than merged using the "Merge channel options". For the quantitative analysis of the p62 aggregates and autophagosomes, every image was thresholded using the "threshold" tool (with a threshold of 100 for the p62 aggregates and 180 for the autophagosomes); subsequently, binary images were inverted, and the number of particles was analysed by the "Analyze Particles" plugin, by setting "size (micron^2)" = from 1 to infinity, and "circularity" = from 0.00 to 1.00. For the brain, particles were analysed on images randomly acquired on whole slices (see the par. *Immunohistochemistry* for details). For cell experiments, particles were analysed for every single cell: the area covered by each cell analysed was manually selected as a region of interest (ROI) on bright-field images (merged with the DAPI signal for tissues and with both the DAPI and the phalloidin signals for cells) and then the ROI was applied to the correspondent p62 positive binary image for the analysis of the particles. Colocalization was evaluated calculating Mander's coefficient with the JACoP plugin in ImageJ as previously done (Galliani et al., 2018). For each graph, images were taken with the same magnification. The confocal settings were kept the same, with pinhole aperture set at 1.0 Airy level and 1024 × 1024 pixels image format for all the experiments.

2.6. Immunoblotting

Western blot was carried out with cultured cells and mouse tissues. For *in vitro* experiments, cells were cultured on standard 6 well plates, treated as previously described, and then lysed on ice with RIPA buffer (R0278-50ML; Sigma Aldrich) containing a protease and phosphatase inhibitors cocktail [cOmplete (4693116001) and PhosSTOP (4906845001); Roche Diagnostics]. Cell lysates were sonicated (for 4 s at 12 μm of intensity) and after centrifugation (15.000 *g* for 25 min, 4 °C) tested for protein concentration by the micro-BCA protein assay kit (23225; Thermo Scientific Pierce). The samples were boiled in Laemli buffer containing β-mercaptoethanol (5% final concentration) for 5 min, centrifuged at room temperature and the supernatants were finally used for gel electrophoresis (SDS-PAGE) or kept at −80 °C until use. For mouse tissues the extracted whole brains and sciatic nerves were lysed on ice with the already mentioned complete RIPA buffer, and homogenized with pestles in 1.5 ml microcentrifuge tubes. Homogenized tissues were then centrifuged (15,000 *g* for 30 min, at 4 °C) and the recovered supernatants were tested for protein content and processed as described above for cell lysates. Samples (6 μg for cell lysates and 30 μg for tissue lysates) were resolved by SDS-PAGE using Gel Criterion XT-Precast polyacrylamide gel 4–12% Bis-Tris (3,450,123; Bio-Rad) and subsequently transferred to nitrocellulose membranes, as previously described (Del Grosso et al., 2016). Immunodetection was performed with the following antibodies: anti-LC3 (1:1000), anti-p62 (1:800; see above for the codes) and anti-Beclin-1 (ab114071; Abcam, 1:1000). On the following day, blots were incubated with the corresponding peroxidase-linked secondary antibodies (goat anti-rabbit or mouse IgG-HRP conjugate; 170-6516 and 170-6515; Biorad, 1:2.500), and after incubation membranes were developed with Clarity enhanced chemiluminescent substrates (1,705,061; Bio-Rad). The chemiluminescent signal was acquired with an ImageQUANT LAS400 scanner (GE Healthcare Life Science), and the density of immunoreactive bands was quantified in ImageJ. Membranes were then incubated with a stripping buffer containing β-mercaptoethanol and re-incubated as above with the anti-tubulin (T6074; Sigma Aldrich; 1:3000) or anti-GADPH (G8795; Sigma Aldrich, 1:3000) for 1 h and then with the corresponding secondary antibodies. Secondary antibody incubation was thus made and images were acquired as described for the primary antibodies. LC3, p62 and Beclin-1 results were normalized to the tubulin content for brain lysates and to GADPH content for fibroblasts, and reported as % of the WT-PND 20 or WT untreated condition respectively.

2.7. PSY quantification

For lipid extraction, WT and TWI cells were plated on standard 60 mm plates. After 48 h of incubation, cells were washed with cold PBS and lysed on ice with 300 µl/well of RIPA buffer containing a protease and phosphatase inhibitors cocktail (as above). For each sample, a mixture was prepared combining the cell lysate, *N*,*N*-dimethylsphingosine 1.250 µM (N,N- DMS, the selected internal standard for LC/MS-MS; SML0311-5MG; Sigma-Aldrich) (Zanfini et al., 2013), and MilliQ water. Then a chloroform/methanol solution (2:1) was added. Samples were vortexed, left at RT for 10 min, and supplemented with NaCl 0.9% *w/v* in Milli-Q water. The biphasic mixture was centrifuged at 800 *g* for 30 min, and the lower layer was collected and evaporated to dryness under vacuum at 30 °C. The residue was dissolved in 50 µl of methanol/formic acid 100/0.1 and processed for HPLC/MS. HPLC/MS quantitation was performed on a Shimadzu Nexera UHPLC chromatograph interfaced with a 5500 QTRAP mass spectrometer (AB SCIEX). HPLC analyses were performed on a Phenomenex Kinetex C8 3 × 150 mm column (particle size 4 µm), using water/methanol/isopropanol/formic acid 40/55/5/0.1 (A) and methanol/isopropanol/formic acid 95/5/0.1 (B) as mobile phases at 0.4 ml/min flow (column temperature = 45 °C). Runs were performed under a 10 min linear gradient from 65 to 100% of solvent B, followed by a 5 min purge step at 100% of B and by a 5 min re-equilibration step to the starting conditions. MRM analyses were performed under the following conditions: ion spray voltage: 5000 V, source temperature 350 °C, declustering potential 50 V, collision energy variable (see value in parentheses), ion source gas 20 l/min, curtain gas: 25 l/min. The following transitions were monitored (acquisition time 150 msec/transition): i) *N*,*N*-dimethylsphingosine (Q1/Q3, *m/z*, CE in parenthesis): 328.2/310.2 (26 V); 328.2/280.2 (32 V); 328.2/110.2 (42 V); ii) PSY (Q1/Q3, m/z, CE in parenthesis): 462.5/444 (25 V); 462.5/282 (30 V);462.5/264 (27 V); 462.5/252 (39 V). Transitions 328.2/310.2 (N,N- dimethylsphingosine) and 462.5/282 (PSY) were used for quantitation purposes.

2.8. Statistical analysis

If not differently specified, data are reported as mean ± SEM obtained from at least three independent experiments (in figure legends, "n" indicates the number of experiments performed). Data were statistically analysed by using Prism 6.00 (GraphPad Software, San Diego, CA; RRID:SCR_002798). For parametric data, Student's *t*-test (unpaired, two-tailed) or one-way ANOVA (Tukey's or Dunnett's multiple-comparisons test) was used; the mean values obtained in each repeated experiment were assumed to be normally distributed about the true mean. Statistical significance refers to results for which $P < .05$ was obtained.

3. Results

3.1. Autophagy is dysregulated in the TWI mouse central and peripheral nervous system

Forasmuch as KD has a strong neurological component, we extensively characterized autophagy in the nervous system of the main KD murine model, the TWI mouse; in particular, the brain and sciatic nerve were chosen as representative components of the central and peripheral nervous system (CNS and PNS), respectively. As markers of autophagy, we focused on p62, LC3 and Beclin-1 (see Introduction for their role in the autophagic flux).

3.1.1. Brain

Immunohistochemistry experiments revealed a markedly increased presence of p62 aggregates (green in Fig. 1 a) in both PND 20 and 30 TWI brains compared to the age-matched WT ones. Quantitative analysis of confocal images, indeed, showed an increase in both their number (Fig. 1 d) and area (Fig. 1 e) in TWI brains. A representative high-magnification image of p62 brain aggregates is also shown in Fig. 1 g. In agreement with these data, western blots reported augmented levels of p62 total expression in TWI brains compared to that measured for WT brains, for PND 20 and PND 30 mice (Fig. 1 h). Taken together, these experiments demonstrate for the first time a general upregulation of the autophagy marker p62 in TWI mice at the early (PND 20) and late stage (PND 30) of the disease. Total LC3 levels, instead, were rather similarly expressed in TWI and WT mice. Fig. 1 a reports representative confocal fluorescence images of total LC3 in TWI and WT brains, for PND 20 and PND 30 mice. No evident differences can be observed by a visual analysis of these images. Quantification of autophagosomes as LC3 positive puncta was then carried out on magnified fluorescence images (Fig. 1 f), and showed no significant variations between TWI and WT mice in both their number and area, in PND 20 and PND 30 brains as well (Fig. 1 b and c). Nevertheless, Western blot data instead highlighted an increased expression of the phosphatidylethanolaminate form of LC3 (LC3-II; Fig. 1 i) in TWI mice with respect to the age-matched WT mice, supporting the hypothesis of upregulation of the autophagy flux. Finally, Beclin-1 total levels were mainly stable among the experimental groups, apart for a slight increase in PND 30 WT brains (Fig. S 1 a), indicating that the initial phase of the autophagy process may not be altered in the TWI brain.

3.1.2. Sciatic nerve

In agreement with the results obtained for the brain, Western blots performed on entire sciatic nerve lysates revealed a very important p62 increase of expression in TWI mice (at both PND 20 and PND 30) compared to the expression found in WT nerves. It was indeed about 3.5 times greater than that of aged matched WT nerves (Fig. 2 a). Similarly, we found upregulation of LC3-II in PND 20 and PND 30 TWI nerves (Fig. 2 b) and, as in the brain, this increase was more evident for late symptomatic mice (PND 30). Moreover, differently to the brain, we reported an increased amount of Beclin-1 in TWI nerves in respect to the WT ones (Fig. S 1 b).

Overall, these experiments demonstrate a widespread up-regulation of the autophagy machinery in the TWI nervous system, which resulted more pronounced in the case of PNS.

3.2. P62 aggregates accumulate differently in distinct neural cell types

In order to investigate the localization of the p62 aggregates we performed a double immunostaining of TWI and WT brain slices with the anti-p62 antibody (red in Fig. 3) together with antibodies specific for different brain cell types (neurons: anti-NeuN, astrocytes: anti-GFAP, oligodendrocytes: anti-MBP; green in Fig. 3). Similarly to what has been previously shown (Fig. 1 a and d), also in this case the WT brain did not highlight significant p62 aggregates; they were instead present in the TWI brain, as expected (Fig. 3 a, b and c). Colocalization was found with the neuronal protein NeuN (Fig. 3 a), a widely used neuronal marker commonly localized in nuclei and perinuclear cytoplasm of most of the neurons in the CNS of mammals (Gusel'Nikova and Korzhevskiy, 2015). Conversely, the glial fibrillary acidic protein (GFAP) did not show colocalization with p62 aggregates (Fig. 3 b). The visual analysis of high magnification images and confocal z-stacks on several GFAP-positive cells, in fact, could not reveal colocalization either in cell nuclei or in cell protrusions. Thus, astrocytes do not seem to be directly involved in the brain accumulations of p62. Finally, Fig. 3 c indicates that colocalization of p62 with oligodendrocytes, marked as MBP-positive cells (Barbarese et al., 1988), also might not occur. However, this is, in our vision, a more ticklish question. As expected, TWI brains presented extended demyelination (Fig. 3 c) due to the characteristic apoptosis of oligodendrocytes that occurs with the disease onset and progression (Graziano and Cardile, 2015; Won et al., 2016). TWI oligodendrocytes differentiation and survival, in fact, are known to be intrinsically defective. These defects are associated with

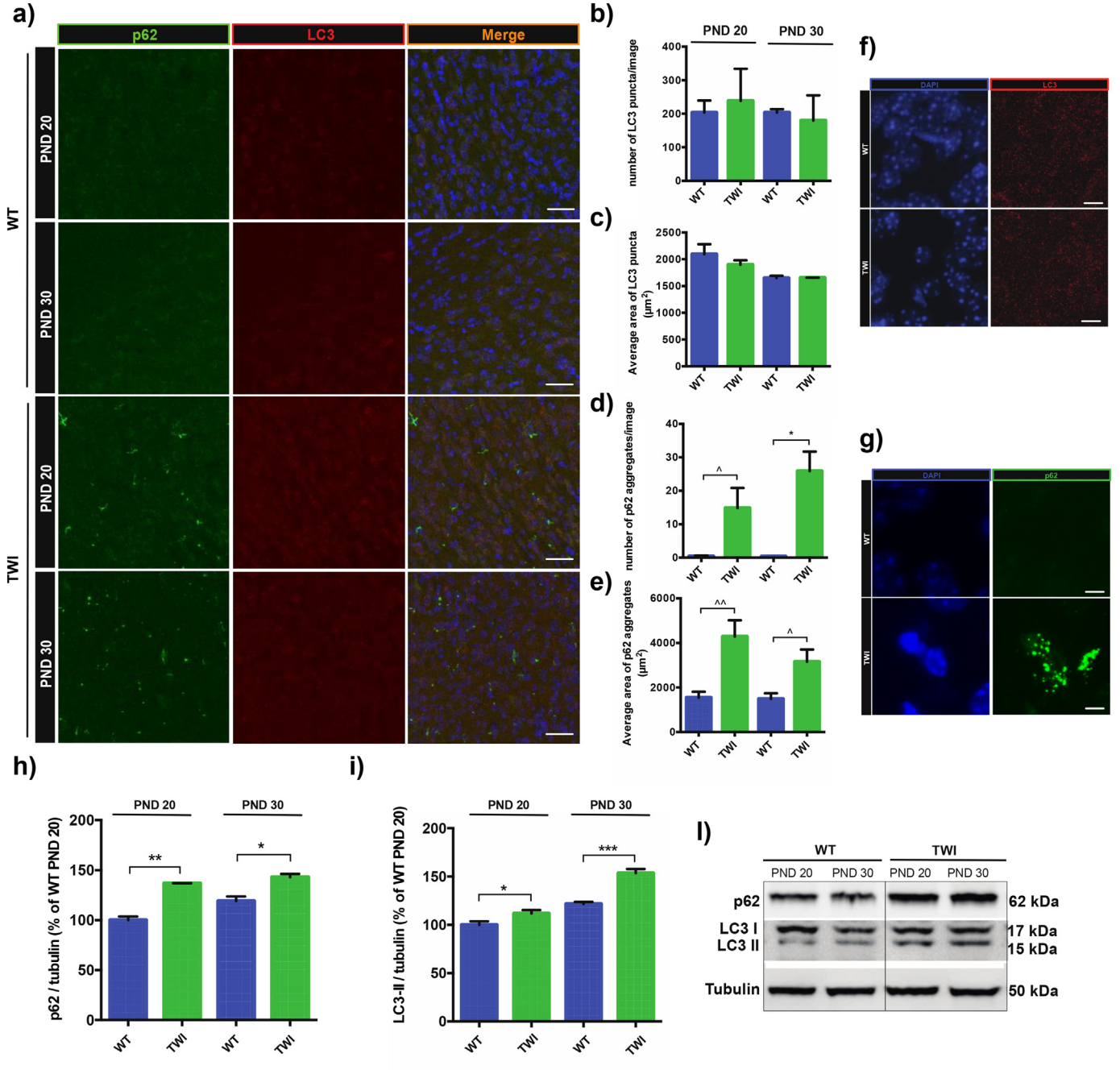

Fig. 1. Autophagy is dysregulated in the TWI brain. (a) Immunohistochemistry staining of WT and TWI brains with anti-p62 (in green) and anti-LC3 (in red) antibodies, nuclei are stained with DAPI (in blue). Scale bar: 37 μm. (b-e) Analysis of the number and average area of LC3 puncta and p62 aggregates per field. (d) p62 aggregates: ^ $P < .15$ TWI-PND20 *vs.* WT-PND 20; * $P < .05$ TWI-PND 30 *vs.* WT-PND 30. (e) Average area of p62 aggregates: ^^ $P < .10$ TWI-PND 20 *vs.* WT-PND 20 and ^ $P < .15$ TWI-PND 30 *vs.* WT-PND 30; Student's *t*-test. Data are shown as mean ± SEM; $n = 4$ WT and n = 4 TWI. (f) High-magnification image of LC3 puncta in WT and TWI brain. Scale bar: 7.5 μm. (g) High-magnification images of p62 aggregates in WT and TWI brain. Scale bar: 7.5 μm. (h) Western blot analysis of the total p62 and LC3-II content in whole brain lysates. (i) p62: ** $P < .01$ TWI-PND 20 *vs.* WT-PND 20; * $P < .05$ TWI-PND 30 *vs.* WT-PND 30. (l) LC3: * $P < .05$ TWI-PND 20 *vs.* WT-PND 20; *** $P < .001$ TWI-PND 30 *vs.* WT-PND 30. Student's t-test. Data are reported as mean ± SEM, $n \geq 3$. (h) Representative western blot bands. (For interpretation of the references to colour in this figure legend, the reader is referred to the web version of this article.)

aberrant accumulation of endogenous PSY and reduced activation of the Erk1/2 and Akt/mTOR pathways before apoptotic cell death (Inamura et al., 2018). Consequently, the scattered and mild fluorescence signal deriving from oligodendrocytes staining made not straightforward the interpretation of colocalization images, and thus assessing the presence of p62 aggregates in oligodendrocytes.

Taken together, these data suggest that p62 accumulation is not homogeneously distributed among different TWI neural cell types. More specifically, while the widespread degeneration of TWI oligodendrocytes made difficult data interpretation for this kind of cells, p62 aggregates were clearly found in neurons, but not in astrocytes.

3.3. Autophagosome-lysosome fusion and autophagosome-mediated p62 recycling are not impaired in TWI brains

We wondered if the p62 accumulations that we found in the TWI

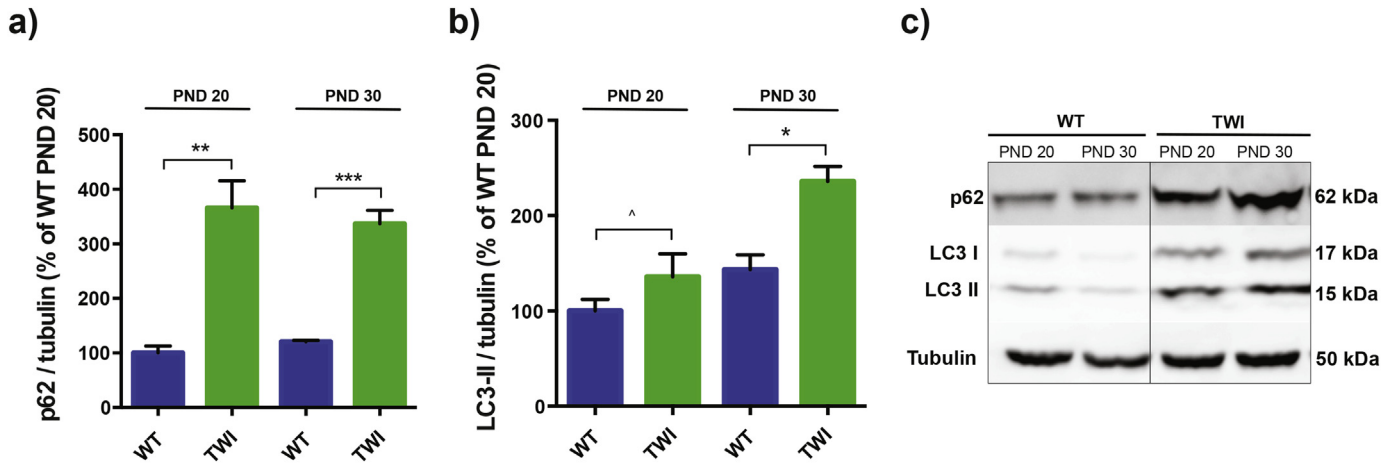

Fig. 2. Autophagy is dysregulated in the TWI sciatic nerve. (a, b) Western blot analysis of the total p62 and LC3-II content in whole sciatic nerve lysates. (a) p62: ** P < .01 TWI-PND 20 *vs.* WT PND 20; *** P < .001 TWI-PND 30 *vs.* WT-PND 30. (b) LC3: ^ *P* = .18 TWI-PND 20 *vs.* WT- PND 20; * P < .05 TWI-PND 30 *vs.* WT-PND 30; Student's t-test. Data are shown as mean ± SEM, n ≥ 3. (c) Representative western blot bands.

brain could be a consequence of an impaired autophagic flux or only the result of an augmented rate of ubiquitinated cell products tagged with p62. To discriminate which of the two hypotheses was correct we performed different double immunostainings to verify the correct progression of some crucial steps of the autophagy pathway.

First, we demonstrated that the autophagy flux correctly reaches its final stage, the fusion of the autophagosome with the lysosome. Colocalization of the autophagosome's marker LC3 with the lysosome's marker LAMP-1 (Settembre et al., 2008b), in fact, occurred in both WT and TWI brains (Fig. 4 a). Mander's colocalization coefficient analysis (LC3/LAMP-1) also revealed higher and less dispersed values for TWI mice with respect to WT mice (Fig. 4 d), suggesting a higher rate of autolysosome formation in the TWI CNS and consequently an increased autophagic activity. We also assayed the colocalization of the p62 aggregates with both autophagosome and lysosome markers, finding that it occurs for both p62 and LAMP-1 (Fig. 4 b and e) and p62 and LC3 (Fig. 4 c and f), in TWI and WT mice as well.

(a) Immunohistochemistry staining of WT and TWI brains with anti-LAMP1 (in red) and anti-LC3 (in green) antibodies, nuclei are stained with DAPI (in blue); scale bar: 2 μm. (b) Immunohistochemistry staining of WT and TWI brains with anti-LAMP1 (in red) and anti-p62 (in green) antibodies (nuclei are stained with DAPI, in blue); scale bar: 10 μm. (c) Immunohistochemistry staining of WT and TWI brains with anti-LC3 (in red) and anti-p62 (in green) antibodies (nuclei are stained with DAPI, in blue); scale bar: 18 μm. (d-f) Mander's coefficients demonstrated that colocalization occurs for LAMP1/LC3, LAMP1/p62 and LC3/p62 in both WT and TWI brains (each point is calculated for a single image). (d) LAMP1/LC3: **** *P* < .0001 TWI *vs.* WT; Student's *t*-test. Mice were sacrificed at PND 20.

3.4. Autophagy is dysregulated in TWI primary cells

In order to better understand if autophagy dysregulation could be determined by the cytotoxic catabolite, PSY, we investigated autophagy in primary fibroblasts from WT and TWI mice, with or without exogenous PSY administration.

For this treatment, we chose the minimum PSY concentration (100 μM) that could diminish cell viability of at least 50% after 24 h from the administration (data not shown). Immunostaining was performed for p62 and LC3, and cells were imaged by confocal fluorescence microscopy (see a representative image in Fig. 5 a). An augmented number of p62 intracellular aggregates was reported in TWI untreated cells and in PSY-treated WT and TWI cells with respect to that measured in WT cells (Fig. 5 c). LC3 puncta, instead, increased only upon PSY treatment, in TWI and WT cells as well; no significant difference was measured between untreated TWI and WT cells (Fig. 5 b). These data agree with what we already observed in a PSY-treated oligodendrocyte cell line (MO3.13) (Del Grosso et al., 2016).

As we did for whole organs extracts, we analysed the total p62 and LC3-II amount in the different conditions by Western blot (Fig. 5 d and e). Total p62 and LC3-II amounts significantly increased in PSY treated cells compared to the untreated ones, both for TWI and for WT cells. We also found higher levels of total p62 for untreated TWI cells with respect to the WT ones. Moreover, to exclude that the measured p62 and LC3-II increase induced by PSY could stem from impaired autophagosome-lysosome fusion rather than from an augmented autophagy activity, we also treated cells with BAF. BAF is a drug that blocks the fusion between lysosomes and autophagosomes and which is typically used to prevent LC3-II and consequently p62 degradation (Del Grosso et al., 2016; Rubinsztein et al., 2009; Singh and Bhaskar, 2018; Mizushima et al., 2010). LC3-II, indeed, is itself degraded by autophagy. By blocking the fusion between autophagosomes and lysosomes, BAF was indeed expected to determine an overall increase of LC3-II in case of functional autophagy.

The administration of BAF induced a further increase of LC3-II and p62 total levels both in presence and absence of GALC activity, proving that enzyme deficiency does not interfere with autophagolysosome formation in our PSY treated cell model (WT + PSY and TWI + PSY). Moreover, the efficacy of BAF has been validated also for untreated WT and TWI cells (WT-UT and TWI-UT; Fig. S2).

We also investigated Beclin-1 expression and found that its main band at 55 kDa (Li et al., 2018) was not statistically different between the distinct WT and TWI conditions, although an increasing trend can be seen in Fig. S 1 d and f. Bands with lower molecular weight appear instead quite different between WT and TWI conditions, showing that the cleavage of the Beclin-1 complex did not occur in the same way in TWI and WT cells (Fig. S 1 e and g).

Finally, in order to assess if the autophagy activation suggested by the increase of p62 expression and number of aggregates per cell in untreated TWI-cells could be attributed to a PSY intracellular accumulation, we quantified the endogenous PSY amount by HPLC/MS in TWI and WT cells. As shown in Fig. 5 g, TWI untreated fibroblasts did not report a significant level of PSY, which was at the limit of detection of our set-up and almost undistinguishable to that measured for WT cells. As a positive control we performed the same measurement in TWI brain lysates. In this case, as expected, PSY resulted well detectable and significantly higher than in WT and TWI fibroblasts. Representative PSY chromatographic peaks are reported in Fig. 5 h, i and l for comparison.

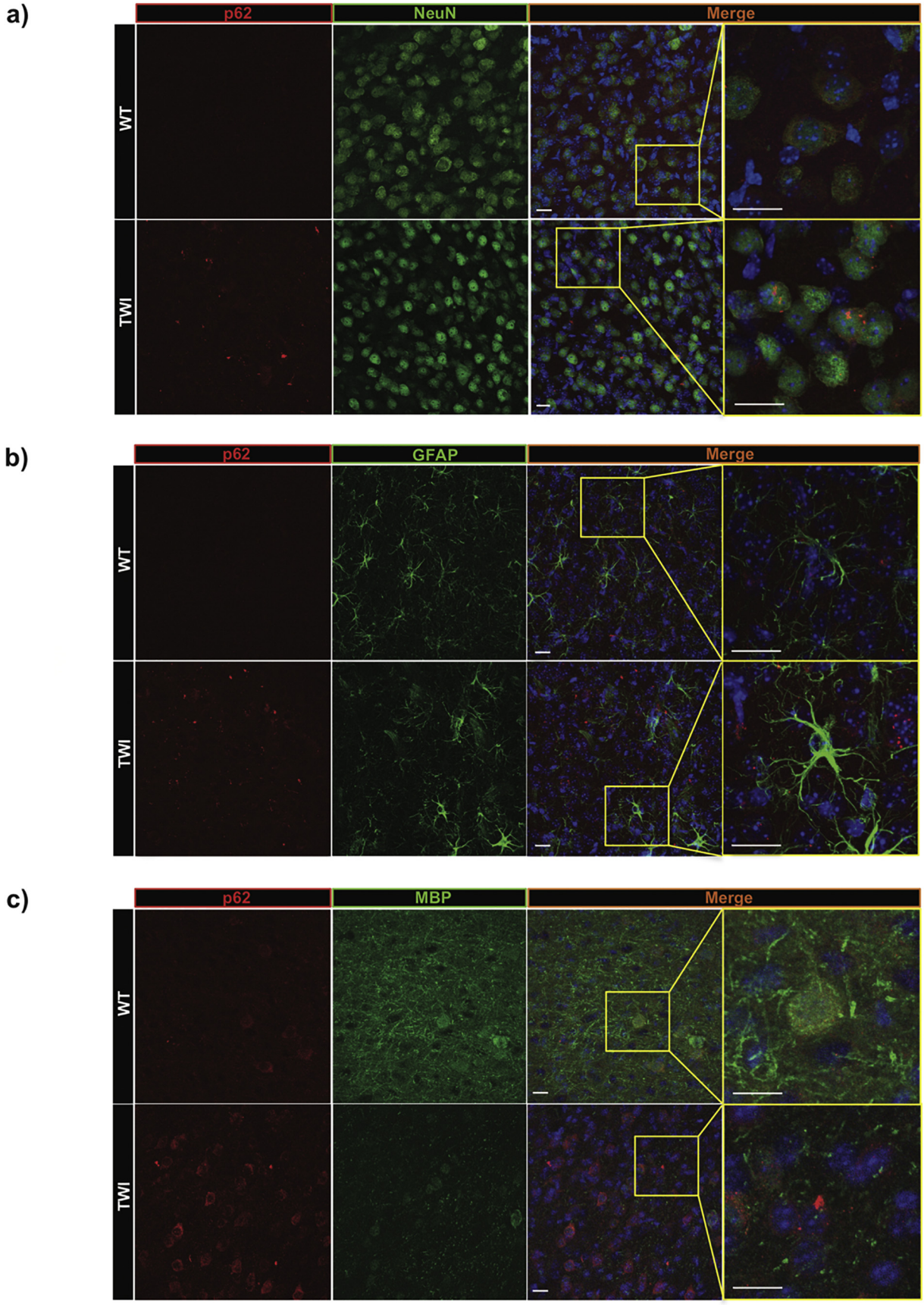

Fig. 3. p62 accumulation in different CNS cell types. Immunohistochemistry staining of WT and TWI brains with anti-p62 antibody (in red) and antibodies for different neuronal cell types (in green): (a) neurons (anti-NeuN), (b) astrocytes (anti-GFAP) and (c) oligodendrocytes (anti-MBP). For every panel (a, b and c) merged images with DAPI (in blue) at normal and 3 X zooms are shown on the right side of the panel. Mice were sacrificed at PND 20. Scale bar: 20 μm.

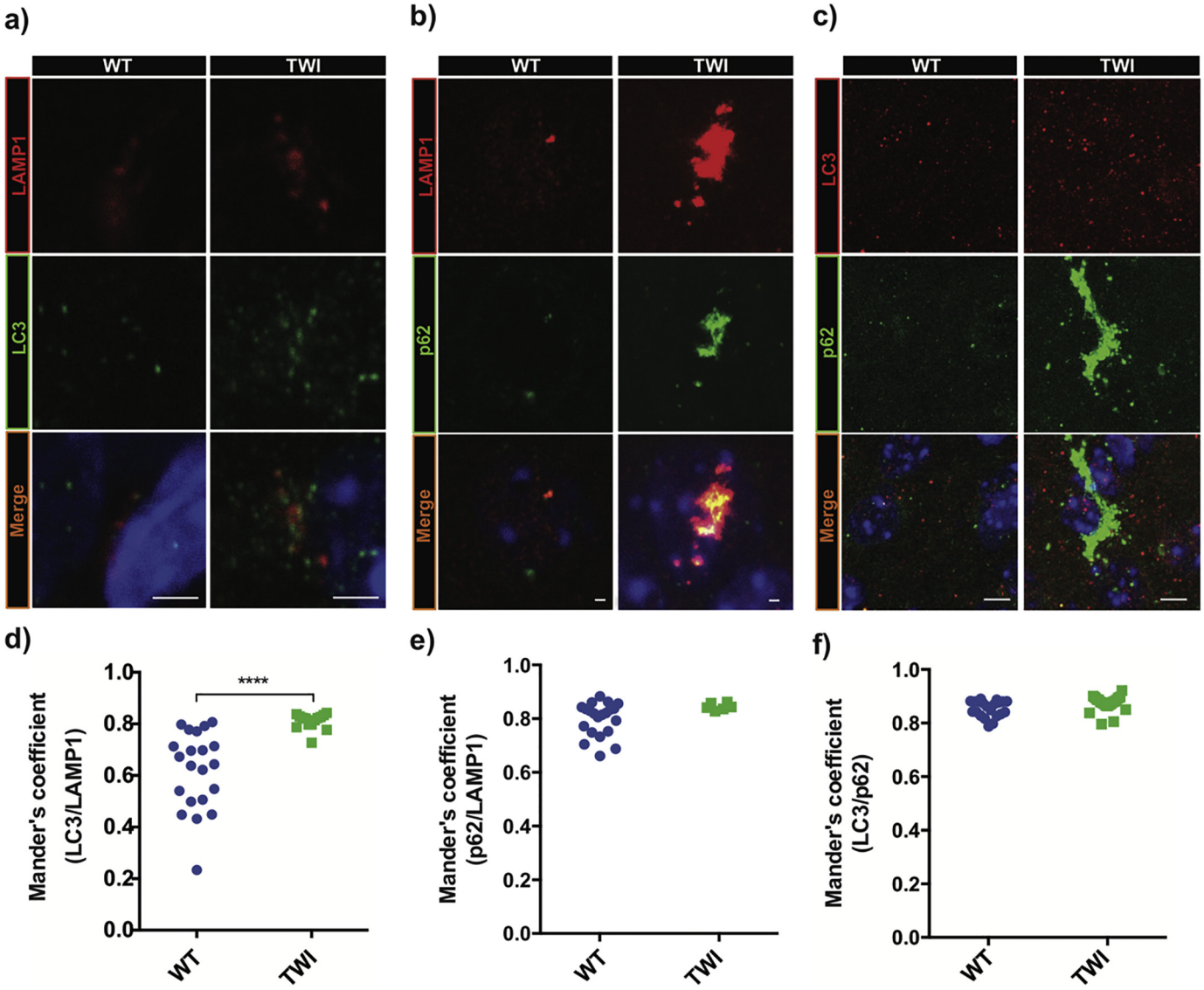

Fig. 4. p62 colocalization with autophagosomes and lysosomes in the TWI brain

3.5. RAP and not RESV-mediated autophagy induction partially restore autophagy markers levels

Given the presence of augmented p62 intracellular aggregates found *in vivo* and *in vitro* in the missing GALC conditions, we decided to test the capability of autophagy inducers to stimulate the clearance of p62-aggregates from cells. We tested two well-known autophagy inducers, RAP and RESV, in TWI cells treated with PSY, so to exacerbate the KD phenotype. The Western blot experiments reported in Fig. 6 a demonstrated that a pre-treatment with RAP before PSY administration can restore the p62 level approximately to that of the wild type. RESV, instead, did not induce relevant changes in the p62 amount in PSY treated cells. LC3-II levels, as expected, increased with the addition of RAP or RESV. In both cases, moreover, p62 and LC3-II levels increased with the addition of BAF, confirming that both RAP and RESV did not impair autolysosome formation in our conditions (Fig. 6 a). Beclin-1, instead, resulted significantly upregulated only in RESV + BAF treated cells (Fig. S 1 f), and, as previously mentioned, TWI and WT cells presented differences in the bands with molecular weights lower than the principal one (55 kDa).

Subsequently we focused on RAP, and studied the number of p62 aggregates and LC3-marked autophagosomes in TWI + PSY cells pre-treated with RAP by immunostaining and confocal fluorescence microscopy (representative images are shown in Fig. 6 d). This experiment confirmed the results obtained with the Western blot analysis, demonstrating that the pre-treatment with RAP can significantly decrease the number of p62 aggregates per cell, bringing back the number of aggregates at an intermediate value between the WT-UT control and the TWI-UT condition (Fig. 6 f). The number of autophagosomes (yellow marked puncta), instead, could not be rescued by RAP pre-treatment (Fig. 6 e).

4. Discussion

KD (GLD; OMIM# 245200) is a rare demyelinating disease belonging to the class of the LSDs. KD results from the deficiency of the lysosomal hydrolase GALC (E.C. 3.2.1.46), that causes the accumulation of the cytotoxic metabolite PSY, one of the β-galactose-containing sphingolipids normally degraded by GALC. PSY accumulation in both CNS and PNS is considered the main cause of KD. In the most recent literature, however, new aspects of the molecular pathogenesis of KD have been discovered, as the involvement of endothelial cell dysfunction in the advancement of the disease (Belleri and Presta, 2016), defects in calcium signalling (Voccoli et al., 2014), the involvement of the

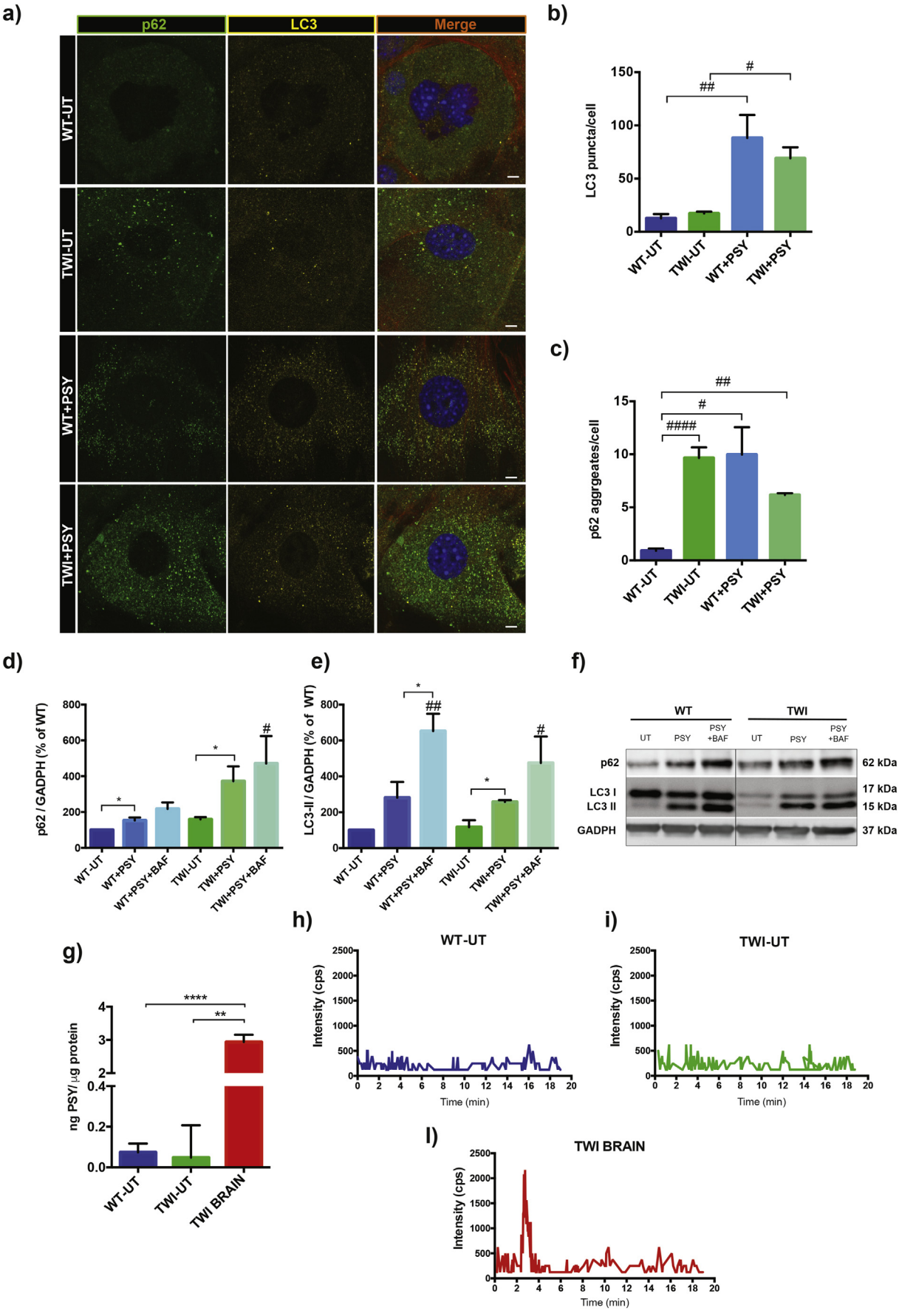

(caption on next page)

Fig. 5. Autophagy in TWI primary cells. (a) Representative confocal imaging of WT and TWI primary fibroblasts treated or not with PSY and immunostained for p62 (in green) and LC3 (in yellow); nuclei are stained with DAPI (in blue) and actin fibers with phalloidin (in red); scale bar: 10 μm. (b, c) Quantification of LC3 and p62 positive puncta. (b) LC3: ## $P < .01$ WT + PSY *vs.* WT-UT, # $P < .05$ TWI + PSY *vs.* TWI-UT; One-way ANOVA, Dunnett's test. (c) p62: #### $P < .0001$ TWI-UT *vs.* WT-UT; # $P < .05$ WT + PSY *vs.* WT-UT; ## $P < .01$ TWI + PSY *vs.* WT-UT; One-way ANOVA, Dunnett's test. Data are shown as mean ± SEM; $n = 3$. (d, e) Western blot analysis of the total p62 and LC3-II content in whole cell lysates. (d) p62: * $P < .05$ WT + PSY and TWI + PSY *vs.* WT-UT and TWI-UT; Student's *t*-test. # $P < .05$ TWI + PSY + BAF *vs.* WT-UT; One-way ANOVA, Dunnett's test. (e) LC3: * $P < .05$ WT + PSY + BAF and TWI + PSY *vs.* WT + PSY and TWI-UT; Student's t-test. # $P < .05$ TWI + PSY + BAF *vs.* WT-UT and ## $P < .01$ WT + PSY + BAF *vs.* WT-UT; One-way ANOVA, Dunnett's test. Data are shown as mean ± SEM; n = 3. (f) Representative western blot bands. (g) HPLC/MS quantification of PSY in WT and TWI primary fibroblast lysates and in a TWI brain (PND 20, used as positive control). (h-l) Representative chromatograms with the PSY monitored transition for quantitative purpose (462.5/282). (For interpretation of the references to colour in this figure legend, the reader is referred to the web version of this article.)

phospholipase A2 in the PSY-induced toxicity (Misslin et al., 2017), and the PSY-induced shedding of membrane microvesicles (D'Auria et al., 2017). Moreover, Nicaise and colleagues (Nicaise et al., 2016), formulated an interesting new hypothesis, “the microglial hypothesis”, which suggests that the pathophysiological effects of PSY could be not only limited to oligodendrocyte death, but rather, PSY may impact primarily on microglia and astrocytes that, when activated, would become cytotoxic for oligodendrocytes. However, the exact pathogenic mechanism that leads from the enzyme deficiency to cell death in KD is still not completely understood and no cure is currently available for KD, being treatment symptomatic and supportive only.

A novelty that could bring freshness to the current therapeutic attempts came with the work of Folts and colleagues. Basically they showed that PSY induces multiple lysosomal dysfunctions (altered lysosomal pH, endolysosomal trafficking, lipid degradation and cathepsin activation), providing for the first time a direct link between enzymatic mutations and lysosomal abnormalities (Folts et al., 2016S). Since cellular waste material, such as proteins or lipids, has to reach lysosomes for degradation in the context of the autophagy pathway, is indeed reasonable to expect autophagy dysfunction to be implicated in the KD pathogenesis. Coupled with the fact that abnormal protein aggregates (*e.g.* α-synuclein and ubiquitinated proteins) have been found in KD brains (Smith et al., 2014; Marshall and Bongarzone, 2016; Abdelkarim et al., 2018), the connection between the autophagy pathway and KD is especially supported. Hence, recent studies focus on the attractive possibility that acting on the autophagic pathway could lead to new promising therapeutic approaches. An example of treatment based on this concept is the idea of restoring physiological lysosomal pH to enhance normal autophagy mediated protein degradation (Guha et al., 2013).

In our previous work, we started investigating autophagy in KD. We demonstrated that autophagy is up-regulated in an oligodendrocyte cell culture upon PSY treatment, and that the further autophagy induction with Lithium is able to ameliorate cell viability after PSY administration. This is, except than for a study performed by Ribbens and colleagues in 2014 (Ribbens et al., 2014), the first time autophagy has been investigated in a KD model. In accordance with our data, they demonstrated *in vitro* that PSY enhances LC3 lysosomal localization and expression in a new GALC-deficient murine oligodendrocyte line.

Here, we focused on the TWI mouse, a naturally occurring model of KD that closely recapitulates most human symptoms. In particular, the TWI mouse functions appear to be normal at birth, symptoms (*e.g.* tremors, muscle weakness in the hindlimbs and decreased body weight) manifest from approximately PND 20, and death occurs near PND 42. In this study, we characterized the expression and localization of some fundamental autophagy markers (p62, LC3 and Beclin-1) in TWI and WT CNS and PNS. We found that the basal levels of autophagy activation are higher in TWI brain and sciatic nerves with respect to the WT ones. At both PND 20 (symptoms onset) and 30 (late stage of the disease), in fact, TWI tissues presented higher levels of LC3-II and p62 and showed increasing trend in Beclin-1 levels especially in the sciatic nerve. Regarding LC3-II, its augmentation positively correlates with increased autophagic activity; at the beginning of autophagosome formation, in fact, LC3 is converted into a cleaved form (LC3-II) and inserted into autophagosome membranes (Eskelinen and Saftig, 2009). Increased brain LC3-II levels have already been found for others lysosomal disorders as Niemman Pick, Sandhoff and GM1 gangliosidosis disease (Boland et al., 2010). For KD, rather, only increased LC3-I expression in the TWI brain has been recently demonstrated (Abdelkarim et al., 2018). p62 aggregates, instead, were not yet reported in literature for KD, but found in many other neurodegenerative and lysosomal disorders models characterized by dysregulated autophagy machinery (Seidel et al., 2017; Micsenyi et al., 2013). Furthermore, we also found that they are clearly present in neurons instead of astrocytes. Thus, accordingly with previous studies indicating that the pathologic process associated with autophagic deficiency is cell-type specific (Komatsu et al., 2007; Smith et al., 2014), these data suggest that there could be a failure in the autophagy process, leading to the accumulation of p62-tagged proteins, which acts differently depending on the cell type. Moreover, these findings suggest that neurodegeneration, classically viewed in KD as a secondary consequence of demyelination, could be reinterpreted as an independent process, that occurs following the accumulation of undigested material, as typically happen in many neurodegenerative disorders (Pierzynowska et al., 2018). Furthermore, reasonably, neurons remain particularly vulnerable to accumulated waste material; given their post-mitotic status, in fact, the possibility of diluting accumulated aggregates is unlikely. Thus, to understand if the accumulation of ubiquitinated undigested material could stem from a defect in the final step of the autophagy pathway, we tested the colocalization of the autophagosomes with the lysosomes, finding that in both WT and TWI brains. Moreover, also p62 colocalizes with both autophagosomes and lysosomes. This indicates that p62 follows the correct steps of the autophagy flux, being first embedded into the autophagosome and subsequently into the lysosome, where predictably is metabolized by lysosomal enzymes. These pieces of evidence suggest that autophagy is dysregulated but not impaired in the TWI brain, thanks to the fact that p62-mediated delivery to the autolysosomes would occur. However, other *in vivo* imaging experiments could be necessary to assess if the amount of autolysosomes is different between healthy and affected mice. Hence, we can speculate that the protein accumulations found in the TWI tissues could be the outcome of a saturated autophagic flux. Specifically, GALC deficiency could lead to a lysosomal dysfunction, partially blocking and, consequently, saturating the autophagy flux. This, in turn, could prevent the degradation of all the p62-tagged material, culminating in aggregations. (Folts et al., 2016).

At this point, we decided to move *in vitro*, where a modulation of the autophagy pathway could be easily implemented. Firstly, we characterized the same autophagy markers also in primary fibroblasts derived from both WT and TWI mice, treated or not with PSY. We demonstrated that PSY administration increased the expression of the autophagy markers LC3-II and p62 in both WT and TWI cells. Beclin-1, instead, appeared to be differently cleaved between WT and TWI cells, indicating a diverse regulation of the early steps of the autophagy machinery. Interestingly, by immunocytochemistry, we also highlighted a higher number of p62 tagged aggregates in the TWI untreated cells with respect to the WT. These data suggest a higher basal level of autophagy activation in the missing GALC condition, that is further stimulated in the presence of PSY. At this point, in order to asses if this difference could be due to the accumulation of endogenous PSY, we

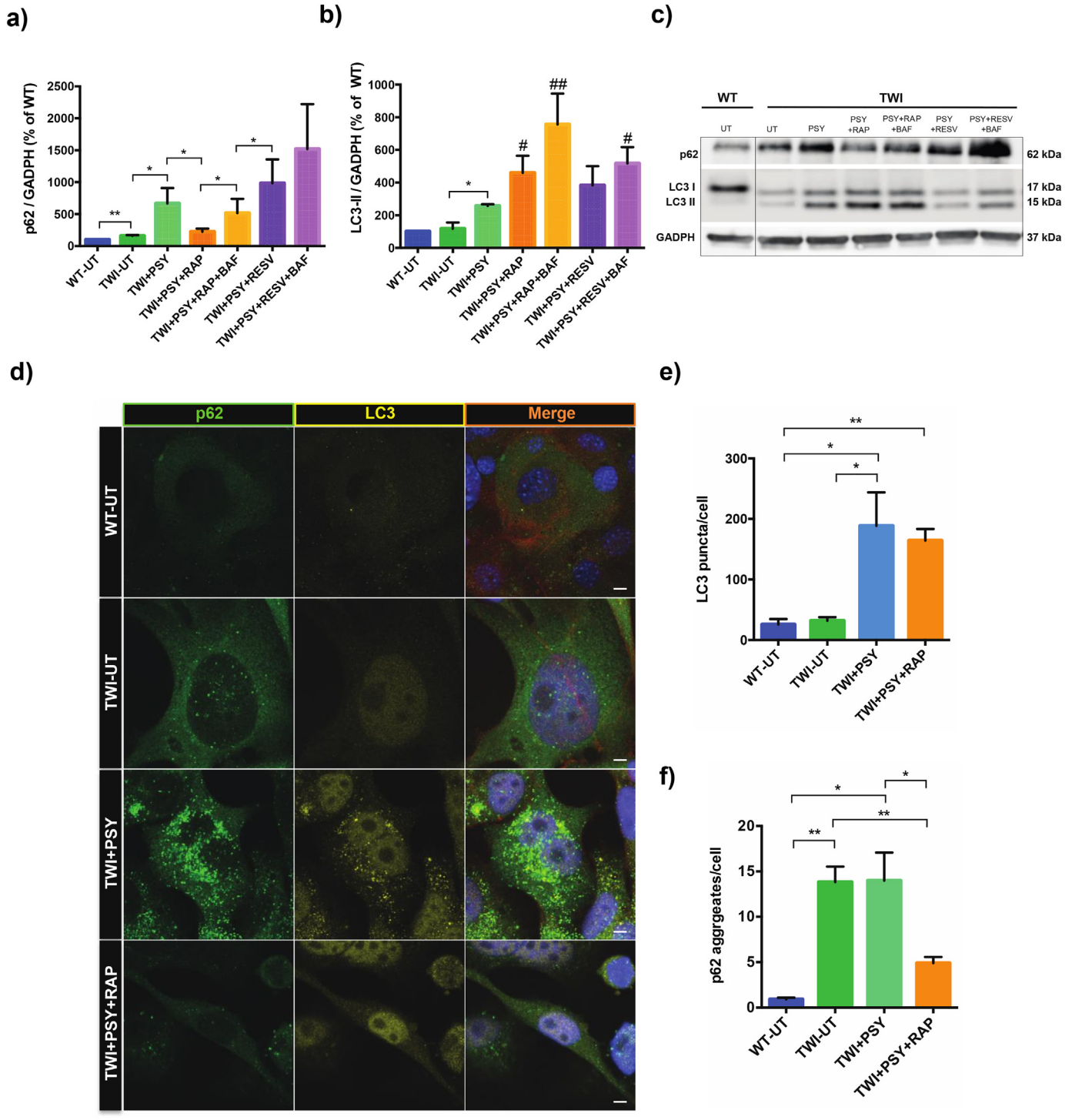

Fig. 6. Autophagy induction in PSY treated primary cells. (a. b) Western blot analysis of the total p62 and LC3-II content in whole cell lysates. (a) p62: * $P < .05$ TWI + PSY *vs.* TWI-UT, TWI + PSY + RAP *vs.* TWI + PSY, TWI + PSY + RAP + BAF *vs.* TWI + PSY + RAP; ** $P < .01$ TWI-UT *vs.* WT-UT. Student's *t*-test. (b) LC3: * P < .05 TWI + PSY *vs.* TWI-UT; Student's t-test. # P < .05 TWI + PSY + RESV + BAF and TWI + PSY + RAP *vs.* WT-UT and ## P < .01 TWI + PSY + RAP + BAF *vs.* WT-UT; One-way ANOVA, Dunnett's test. Data are shown as mean ± SEM; $n = 3$. (c) Representative western blot bands. (d) Immunocytochemistry staining of WT and TWI primary fibroblasts treated or not with PSY and RAP, immunostained for LC3 (in yellow) and p62 (in green); nuclei are stained with DAPI (in blue) and actin fibers with phalloidin (in red); scale bar: 10 μm. (e, f) Quantification of LC3 puncta and p62 aggregates. (e) LC3: * P < .05 TWI + PSY *vs.* WT-UT and TWI-UT; ** P < .01 TWI + PSY + RAP *vs.* WT-UT. (f) p62: ** P < .01 TWI-UT *vs.* WT-UT and TWI + PSY + RAP *vs.* TWI-UT; * P < .05 TWI + PSY *vs.* WT-UT and TWI + PSY + RAP *vs.* TWI + PSY. Student's t-test. Data are shown as mean ± SEM; n = 3. (For interpretation of the references to colour in this figure legend, the reader is referred to the web version of this article.)

quantified it by HPLC/MS. Given the lack of PSY content in both WT and TWI cells, we hypothesized that, probably, some other molecular mechanism, not directly linked with PSY accumulation, should be considered. A hydrolase deficiency, in fact, as commonly happens in LSDs, cause a general imbalance in the lysosome homeostasis, preventing the development of an optimal environment for the correct recycling of all the waste material. Besides the already demonstrated PSY-induced autophagy activation (Del Grosso et al., 2016), thus, also the GALC deficiency would be responsible for the increased autophagic flux in an at least partially PSY-independent manner. Subsequently, aiming to promote the clearance of the p62 tagged aggregates and thus rescue the WT phenotype, we tested *in vitro* two well-known autophagy inducers (RAP and RESV). Both the modulators, as expected, activated the autophagy flow in our cellular model. Furthermore, while RESV did not reduce the p62 intracellular levels, RAP rescued the WT levels of the total p62 expression in cells disturbed by the presence of PSY. Moreover, the number of aggregates showed a significant reduction, partially restoring the WT condition. Given the presence of a wide recent literature showing the positive effect of autophagy induction on the clearance of accumulated cell aggregates *in vitro* (Ravikumar et al., 2002; Sarkar and Rubinsztein, 2008; Webb et al., 2003), our results concerning the reduction of aggregates after the RAP-mediated autophagy induction is not surprising. Thus, our data strongly give the rationale to test autophagy induction in the TWI mouse to remove protein aggregates from the nervous system. Moreover, since RAP is already available as pharmaceutical preparations, in case of positive *in vivo* results, this therapy could also be readily applicable to humans for clinical testing.

Although additional studies are required to fully characterize the autophagy machinery in the TWI mice, this paper suggests autophagy dysregulation as a new aspect involved in the molecular pathogenesis of KD. This could at least partially explain the failure of the main therapeutic attempts in completely curing this LSD. Despite important advances made in the last years in research, in fact, the principally studied therapies (as BMT, gene/cell therapy and their combination) can increase life expectancy of the treated TWI mice, which, however, later suddenly die for unclear complications (Rafi et al., 2015; Ricca et al., 2015). This late death may be due to additional pathological processes that proceed despite the GALC provision. Therefore, autophagy modulation could be a promising option to be tested in combination with a main GALC-deficiency correcting therapy (as gene therapy and/or enzyme replacement therapy) to help in achieving a complete KD phenotype rescue.

Acknowledgments

This research was supported by: Fondazione Cassa Di Risparmio di Lucca under the framework of the project “Pre-Clinical Testing of Lithium Treatment in Krabbe Disease”; European Leukodystrophy Association (ELA) International, under the framework of the project “Development of a novel, nanovector-mediated enzyme replacement therapy for Globoid Cell Leukodystrophy (GLD)”, Grant no. ELA 2015-010C1A.

Appendix A. Supplementary data

Supplementary data to this article can be found online at https://doi.org/10.1016/j.nbd.2019.05.011.

References

Abdelkarim, H., Marshall, M.S., Scesa, G., Smith, R.A., Rue, E., Marshall, J., et al., 2018. α-Synuclein interacts directly but reversibly with psychosine: implications for α-synucleinopathies. Sci. Rep. 8 (1), 12462.

Ballabio, A., Gieselmann, V., 2009. Lysosomal disorders: from storage to cellular damage. Biochim. Biophys. Acta (BBA)-Mol. Cell Res. 1793 (4), 684–696.

Barbarese, E., Barry, C., Chou, C.H.J., Goldstein, D.J., Nakos, G.A., Hyde-DeRuyscher, R., 1988. Expression and localization of myelin basic protein in oligodendrocytes and transfected fibroblasts. J. Neurochem. 51 (6), 1737–1745.

Belleri, M., Presta, M., 2016. Endothelial cell dysfunction in globoid cell leukodystrophy. J. Neurosci. Res. 94 (11), 1359–1367.

Boland, B., Smith, D.A., Mooney, D., Jung, S.S., Walsh, D.M., Platt, F.M., 2010. Macroautophagy is not directly involved in the metabolism of amyloid precursor protein. J. Biol. Chem. 285, 37415–37426. https://doi.org/10.1074/jbc.M110.186411. (jbc-M110).

Cappello, V., Marchetti, L., Parlanti, P., Landi, S., Tonazzini, I., Cecchini, M., et al., 2016. Ultrastructural characterization of the lower motor system in a mouse model of Krabbe disease. Sci. Rep. 6 (1), 1.

D'Auria, L., Reiter, C., Ward, E., Moyano, A.L., Marshall, M.S., Nguyen, D., 2017. Psychosine enhances the shedding of membrane microvesicles: implications in demyelination in Krabbe's disease. PLoS One 12 (5), e0178103.

de Vito, G., Tonazzini, I., Cecchini, M., Piazza, V., 2014. RP-CARS: label-free optical readout of the myelin intrinsic healthiness. Opt. Express 22 (11), 13733–13743.

de Vito, G., Cappello, V., Tonazzini, I., Cecchini, M., Piazza, V., 2017. RP-CARS reveals molecular spatial order anomalies in myelin of an animal model of Krabbe disease. J. Biophotonics 10 (3), 385–393.

Del Grosso, A., Antonini, S., Angella, L., Tonazzini, I., Signore, G., Cecchini, M., 2016. Lithium improves cell viability in psychosine-treated MO3. 13 human oligodendrocyte cell line via autophagy activation. J. Neurosci. Res. 94 (11), 1246–1260.

Duchen, L.W., Eicher, E.M., Jacobs, J.M., Scaravilli, F., Teixeira, F., 1980. Hereditary leucodystrophy in the mouse: the new mutant twitcher. Brain J. Neurol. 103 (3), 695–710.

Esch, S.W., Williams, T.D., Biswas, S., Chakrabarty, A., Levine, S.M., 2003. Sphingolipid profile in the CNS of the twitcher (globoid cell leukodystrophy) mouse: a lipidomics approach. Cell. Mol. Biol. (Noisy-le-Grand, France) 49 (5), 779–787.

Eskelinen, E.L., Saftig, P., 2009. Autophagy: a lysosomal degradation pathway with a central role in health and disease. Biochim. Biophys. Acta (BBA)-Mol. Cell Res. 1793 (4), 664–673.

Fleming, A., Noda, T., Yoshimori, T., Rubinsztein, D.C., 2011. Chemical modulators of autophagy as biological probes and potential therapeutics. Nat. Chem. Biol. 7 (1), 9.

Floden, A.M., Combs, C.K., 2011. Microglia demonstrate age-dependent interaction with amyloid-β fibrils. J. Alzheimers Dis. 25 (2), 279–293.

Folts, C.J., Scott-Hewitt, N., Pröschel, C., Mayer-Pröschel, M., Noble, M., 2016. Lysosomal re-acidification prevents lysosphingolipid-induced lysosomal impairment and cellular toxicity. PLoS Biol. 14 (12), e1002583.

Fu, R., Mei, Q., Zuo, W., Li, J., Gregor, D., Bekker, A., Ye, J., 2017. Low-dose ethanol excites lateral habenula neurons projecting to VTA, RMTg, and raphe. Int. J. Physiol. Pathophysiol. Pharmacol. 9 (6), 217.

Galliani, M., Santi, M., Del Grosso, A., Cecchettini, A., Santorelli, F.M., Hofmann, S.L., 2018. Cross linked enzyme aggregates as versatile tool for enzyme delivery: application to polymeric nanoparticles. Bioconjug. Chem. 29 (7), 2225–2231. https://doi.org/10.1021/acs.bioconjchem.8b00206.

Ghaiad, H.R., Nooh, M.M., El-Sawalhi, M.M., Shaheen, A.A., 2016. Resveratrol promotes remyelination in cuprizone model of multiple sclerosis: biochemical and histological study. Mol. Neurobiol. 54 (5), 3219–3229.

Graziano, A.C.E., Cardile, V., 2015. History, genetic, and recent advances on Krabbe disease. Gene 555 (1), 2–13.

Guha, S., Baltazar, G.C., Coffey, E.E., Tu, L.A., Lim, J.C., Beckel, J.M., 2013. Lysosomal alkalinization, lipid oxidation, and reduced phagosome clearance triggered by activation of the P2X7 receptor. FASEB J. 27 (11), 4500–4509.

Gusel'Nikova, V.V., Korzhevskiy, D.E., 2015. NeuN as a neuronal nuclear antigen and neuron differentiation marker. Acta Nat. 7 (2), 25 (англоязычная версия).

Inamura, N., Kito, M., Go, S., Kishi, S., Hosokawa, M., Asai, K., Takakura, N., Takebayashi, H., Matsuda, J., Enokido, Y., 2018. Developmental defects and aberrant accumulation of endogenous psychosine in oligodendrocytes in a murine model of Krabbe disease. Neurobiol. Dis. 120, 51–62.

Kang, R., Zeh, H.J., Lotze, M.T., Tang, D., 2011. The Beclin 1 network regulates autophagy and apoptosis. Cell Death Differ. 18 (4), 571.

Komatsu, M., Waguri, S., Koike, M., Sou, Y.S., Ueno, T., Hara, T., 2007. Homeostatic levels of p62 control cytoplasmic inclusion body formation in autophagy-deficient mice. Cell 131 (6), 1149–1163.

Li, F., Zhang, C., Li, Y., Hou, X., Zhou, X., Wang, A., 2018. Beclin1 restricts RNA virus infection in plants through suppression and degradation of the viral polymerase. Nat. Commun. 9 (1), 1268.

Lieberman, A.P., Puertollano, R., Raben, N., Slaugenhaupt, S., Walkley, S.U., Ballabio, A., 2012. Autophagy in lysosomal storage disorders. Autophagy 8 (5), 719–730.

Lu, Y., Lin, B., Zhong, J., 2017. The therapeutic effect of dexmedetomidine on rat diabetic neuropathy pain and the mechanism. Biol. Pharm. Bull. 40 (9), 1432–1438.

Mandrioli, J., D'Amico, R., Zucchi, E., Gessani, A., Fini, N., Fasano, A., 2018. Rapamycin treatment for amyotrophic lateral sclerosis: protocol for a phase II randomized, double-blind, placebo-controlled, multicenter, clinical trial (RAP-ALS trial). Medicine 97 (24), e11119.

Marshall, M.S., Bongarzone, E.R., 2016. Beyond Krabbe's disease: the potential contribution of galactosylceramidase deficiency to neuronal vulnerability in late-onset synucleinopathies. J. Neurosci. Res. 94 (11), 1328–1332.

Micsenyi, M.C., Sikora, J., Stephney, G., Dobrenis, K., Walkley, S.U., 2013. Lysosomal membrane permeability stimulates protein aggregate formation in neurons of a lysosomal disease. J. Neurosci. 33 (26), 10815–10827.

Mikulka, C.R., Sands, M.S., 2016. Treatment for Krabbe's disease: finding the combination. J. Neurosci. Res. 94 (11), 1126–1137.

Misslin, C., Velasco-Estevez, M., Albert, M., Albert, M., O'Sullivan, S.A., Dev, K.K., 2017. Phospholipase A2 is involved in galactosylsphingosine-induced astrocyte toxicity, neuronal damage and demyelination. PLoS One 12 (11), e0187217.

Mizushima, N., Yoshimori, T., Levine, B., 2010. Methods in mammalian autophagy research. Cell 140 (3), 313–326.
Nicaise, A.M., Bongarzone, E.R., Crocker, S.J., 2016. A microglial hypothesis of globoid cell leukodystrophy pathology. J. Neurosci. Res. 94 (11), 1049–1061.
Pan, T., Kondo, S., Zhu, W., Xie, W., Jankovic, J., Le, W., 2008. Neuroprotection of rapamycin in lactacystin-induced neurodegeneration via autophagy enhancement. Neurobiol. Dis. 32 (1), 16–25.
Parlanti, P., Cappello, V., Brun, F., Tromba, G., Rigolio, R., Tonazzini, I., 2017. Size and specimen-dependent strategy for x-ray micro-ct and tem correlative analysis of nervous system samples. Sci. Rep. 7 (1), 2858.
Pellegrini, D., del Grosso, A., Angella, L., Giordano, N., Dilillo, M., Tonazzini, .I, Caleo, M., Cecchini, M., McDonnel, L., 2019. Quantitative Microproteomics Based Characterization of the Central and Peripheral Nervous System of a Mouse Model of Krabbe Disease. Mol. Cell Proteomicshttps://doi.org/10.1074/mcp.RA118.001267. mcp. RA118. 001267.
Pierzynowska, K., Gaffke, L., Cyske, Z., Puchalski, M., Rintz, E., Bartkowski, M., 2018. Autophagy stimulation as a promising approach in treatment of neurodegenerative diseases. Metab. Brain Dis. 1–20.
Rafi, M.A., Rao, H.Z., Luzi, P., Wnger, D.A., 2015. Long-term improvements in lifespan and pathology in CNS and PNS after BMT plus one intravenous injection of AAVrh10-GALC in twitcher mice. Mol. Ther. 23 (11), 1681–1690.
Ravikumar, B., Duden, R., Rubinsztein, D.C., 2002. Aggregate-prone proteins with polyglutamine and polyalanine expansions are degraded by autophagy. Hum. Mol. Genet. 11 (9), 1107–1117.
Ravikumar, B., Vacher, C., Berger, Z., Davies, J.E., Luo, S., Oroz, L.G., et al., 2004. Inhibition of mTOR induces autophagy and reduces toxicity of polyglutamine expansions in fly and mouse models of Huntington disease. Nat. Genet. 36 (6), 585.
Ribbens, J.J., Moser, A.B., Hubbard, W.C., Bongarzone, E.R., Maegawa, G.H., 2014. Characterization and application of a disease-cell model for a neurodegenerative lysosomal disease. Mol. Genet. Metab. 111 (2), 172–183.
Ricca, A., Rufo, N., Ungari, S., Morena, F., Martino, S., Kulik, W., et al., 2015. Combined gene/cell therapies provide long-term and pervasive rescue of multiple pathological symptoms in a murine model of globoid cell leukodystrophy. Hum. Mol. Genet. 24 (12), 3372–3389.
Rubinsztein, D.C., Cuervo, A.M., Ravikumar, B., Sarkar, S., Korolchuk, V.I., Kaushik, S., Klionsky, D.J., 2009. In search of an “autophagomometer”. Autophagy 5 (5), 585–589.
Rubinsztein, D.C., Codogno, P., Levine, B., 2012. Autophagy modulation as a potential therapeutic target for diverse diseases. Nat. Rev. Drug Discov. 11 (9), 709.
Sakai, N., Inui, K., Tatsumi, N., Fukushima, H., Nishigaki, T., Taniike, M., 1996. Molecular cloning and expression of cDNA for murine galactocerebrosidase and mutation analysis of the twitcher mouse, a model of Krabbe's disease. J. Neurochem. 66 (3), 1118–1124.
Sarkar, S., Rubinsztein, D.C., 2008. Huntington's disease: degradation of mutant huntingtin by autophagy. FEBS J. 275 (17), 4263–4270.
Sarkar, S., Ravikumar, B., Rubinsztein, D.C., 2009. Autophagic clearance of aggregate-prone proteins associated with neurodegeneration. Methods Enzymol. 453, 83–110.
Seidel, K., Siswanto, S., Fredrich, M., Bouzrou, M., den Dunnen, W.F., Özerden, I., 2017. On the distribution of intranuclear and cytoplasmic aggregates in the brainstem of patients with spinocerebellar ataxia type 2 and 3. Brain Pathol. 27 (3), 345–355.
Settembre, C., Fraldi, A., Rubinsztein, D.C., Ballabio, A., 2008a. Lysosomal storage diseases as disorders of autophagy. Autophagy 4 (1), 113–114.
Settembre, C., Fraldi, A., Rubinsztein, D.C., Ballabio, A., 2008b. Lysosomal storage diseases as disorders of autophagy. Autophagy 4 (1), 113–114.
Singh, B., Bhaskar, S., 2018. Methods for detection of autophagy in mammalian cells. Methods Mol. Biol. 1, 14.
Smith, B.R., Santos, M.B., Marshall, M.S., Cantuti-Castelvetri, L., Lopez-Rosas, A., Li, G., et al., 2014. Neuronal inclusions of α-synuclein contribute to the pathogenesis of Krabbe disease. J. Pathol. 232 (5), 509–521.
Spalletti, C., Alia, C., Lai, S., Panarese, A., Conti, S., Micera, S., Caleo, M., 2017. Combining robotic training and inactivation of the healthy hemisphere restores pre-stroke motor patterns in mice. Elife 6, e28662.
Tonazzini, I., Jacchetti, E., Meucci, S., Beltram, M., Cecchini, M., 2015. Schwann cell contact guidance versus boundary interaction in functional wound healing along nano and microstructured membranes. Adv. Healthcare Mater. 4 (12), 1849–1860.
Voccoli, V., Tonazzini, I., Signore, G., Caleo, M., Cecchini, M., 2014. Role of extracellular calcium and mitochondrial oxygen species in psychosine-induced oligodendrocyte cell death. Cell Death Dis. 5 (11), e1529.
Wang, T., Lao, U., Edgar, B.A., 2009. TOR-mediated autophagy regulates cell death in Drosophila neurodegenerative disease. J. Cell Biol. 186 (5), 703–711.
Webb, J.L., Ravikumar, B., Atkins, J., Skepper, J.N., Rubinsztein, D.C., 2003. α-Synuclein is degraded by both autophagy and the proteasome. J. Biol. Chem. 278 (27), 25009–25013.
Whitfield, P.D., Sharp, P.C., Taylor, R., Meikle, P., 2001. Quantification of galactosylsphingosine in the twitcher mouse using electrospray ionization-tandem mass spectrometry. J. Lipid Res. 42 (12), 2092–2095.
Won, J.S., Singh, A.K., Singh, I., 2016. Biochemical, cell biological, pathological, and therapeutic aspects of K rabbe's disease. J. Neurosci. Res. 94 (11), 990–1006.
Zanfini, A., Dreassi, E., Berardi, A., Governini, L., Corbini, G., Costantino-Ceccarini, E., 2013. Quantification of psychosine in the serum of twitcher mouse by LC–ESI-tandem-MS analysis. J. Pharm. Biomed. Anal. 80, 44–49.